Large Eddy Simulations of Model-Scale Turbulent Atmospheric Boundary Layer Flows

Liang Shi[1] and DongHun Yeo, M.ASCE[2]

Abstract: This paper presents large eddy simulations (LES) of model-scaled neutrally stratified atmospheric boundary layer (ABL) flows for structural engineering applications and examines their statistical properties. A one-k-equation eddy model is used for the subgrid-scale (SGS) motions, and a wall shear model is applied on the ground. The mean streamwise velocity profile is approximately logarithmic, yet near the ground a mismatch persists because of the limited accuracy of the SGS model. The second moments of the turbulence represent well the underlying physics. The spectra of the velocity components at a point are consistent with commonly accepted expressions. The spatial coherences decay exponentially as functions of reduced frequencies. The results suggest that, except for the mean velocity near the ground, the ABL turbulence statistics can be well represented by large eddy simulations with simple SGS and wall models. **DOI: 10.1061/(ASCE)EM.1943-7889.0001281.**

Author keywords: Atmospheric boundary layer; Large eddy simulations; Turbulence.

Introduction

An accurate representation of atmospheric boundary layer (ABL) turbulence is needed to estimate wind loads on buildings. To evaluate the performance of current open-source computational fluid dynamics (CFD) capabilities in computational wind engineering applications, *OpenFOAM* is used in this paper to conduct large eddy simulations (LES) simulations of ABL flow. The statistical properties of the flow obtained in the simulations includes the mean velocity profile, the shear stresses, the spectral density, and spatial coherence of velocity fluctuations, which has rarely been examined by CFD practitioners but plays a significant role in building design. The results of the simulations are compared with theoretical results or commonly accepted expressions. Simulation details are described first. The turbulence statistics are presented next, followed by conclusions.

Simulation Details

The ABL height is assumed to be 1 km, and the terrain roughness for open terrain exposure is assumed to be 0.03 m. The ultimate goal is to determine the extent to which CFD simulations are comparable to conventional wind-tunnel simulations in air at length scales of the order of 1:1,000 and velocity scales of approximately 1:5. For this reason, simulations were performed at the same length and velocity scales and the same kinematic viscosity as for the wind tunnel simulations. The Reynolds number violation inherent in the CFD simulation and in typical wind tunnel simulations of the ABL flow are therefore the same. The mean along-wind velocity at the top of the computational domain, u_{ref}, is assumed to be 10 m/s. The kinematic viscosity of the air at 15°C and sea level is $\nu = 1.455 \times 10^{-5}\ \text{m}^2/\text{s}$. The surface friction velocity is $u_* = \kappa u_{\text{ref}}/\ln(H/z_0) \simeq 0.394\ \text{m/s}$, and the von Kármán constant κ is assumed to be 0.41.

The dimensions in the streamwise and spanwise direction are $L_x \times L_y = 2H \times H$. Periodic boundary conditions are imposed in the horizontal directions. For velocity, the no-slip boundary condition is applied on the ground, whereas the slip condition is applied at the top, that is, zero normal velocity and zero-gradient tangential velocity. For the pressure field, a zero-gradient boundary condition is imposed at both the ground and the top. The instantaneous wall shear model, originally introduced by Schumann (1975) and based on local equilibrium in the near-wall region, is applied at the ground level. For details, see Shi and Yeo (2016).

All the simulations are performed with *OpenFOAM* (version 2.4.0). The solver used in this paper is a modified form of the standard solver *pimpleFOAM*, based on a merged pressure-implicit split operator (PISO) and semi-implicit method for pressure-linked equations (SIMPLE) algorithm (Jasak 1996). An external constant force F is added to the x-component differential equation, and most of the horizontally averaged statistics are generated in runtime. This solver allows dynamically adjusting the time step in runtime based on the specified maximum Courant-Friedrichs-Lewy (CFL) number (Courant et al. 1928) (CFL = 0.25 in the simulations), which reduces the initial relaxation time. However, at the stationary state, the time step is fixed to be $\Delta t = 0.00025$ s. The time discretization is performed by the implicit Crank-Nicolson scheme (Crank and Nicolson 1947) with a coefficient of 0.9. The Gaussian-type schemes are chosen for the spatial (gradient, divergence, and Laplacian) discretization. The Poisson equation for pressure is solved by generalized the geometric-algebraic multigrid (GAMG) algorithm, and the linear equation for velocity is solved by the preconditioned biconjugate gradient (PBiCG) algorithm. Linear interpolation is used to obtain the physical quantities at the surface centers of the cells. Mesh is generated by the utility blockMesh in *OpenFOAM*. The total number of cells is $N_x \times N_y \times N_z = 200 \times 100 \times 100 = 2$ million. The grid is uniform, equidistant in all directions ($\Delta z = 0.01H$), which removes the commuting errors of the LES filtering operator for nonuniform grids. The

[1]NIST Director's Postdoctoral Fellow, Engineering Laboratory, National Institute of Standards and Technology, Gaithersburg, MD 20899. ORCID: http://orcid.org/0000-0002-2658-7837

[2]IPA Research Engineer, Engineering Laboratory, National Institute of Standards and Technology, Gaithersburg, MD 20899 (corresponding author). E-mail: donghun.yeo@nist.gov

Note. This manuscript was submitted on May 13, 2016; approved on February 7, 2017; published online on May 9, 2017. Discussion period open until October 9, 2017; separate discussions must be submitted for individual papers. This technical note is part of the ***Journal of Engineering Mechanics***, © ASCE, ISSN 0733-9399.

one-k-equation (oneEqEddy) model in *OpenFOAM v2.4.0* is used. Simulations were performed until the statistical states are stationary, and then data was sampled for $1{,}000\tau_H$, i.e., approximately 800 turnovers at $z = 0.1H$.

Results

Mean Velocity

In the surface layer of ABL flow ($z/H \lesssim 0.1$), the mean wind velocity follows approximately a logarithmic profile, $\langle u \rangle = u_* \ln(z/z_0)/\kappa$. The underlying assumptions are the Boussinesq approximation and the Prandtl mixing-length hypothesis. The Boussinesq approximation connects the Reynolds stress to the mean shear through the eddy viscosity ν_T, $-\langle u'w' \rangle = \nu_T \, d\langle u \rangle/dz$, while ν_T is further estimated by surface velocity u_* and the Prandtl mixing-length scale κz, $\nu_T = u_* \kappa z$. In the flow, the Reynolds stress is balanced approximately by the wall shear, which leads to the $-\rho u_*^2 = -\rho u_* \kappa z \, d\langle u \rangle/dz$. The preceding log-law profile is obtained by solving this equation with the no-slip boundary condition at the aerodynamic roughness height z_0. Because of the imposed constant external pressure gradient, the logarithmic profile is expected to hold for the whole ABL height. The profile from the simulation deviates by up to 10% from the logarithmic profile, owing largely to the inaccuracy of the subgrid-scale (SGS) model near the ground, where the flow is anisotropic and inhomogeneous. The other two velocity components, $\langle v \rangle$ and $\langle w \rangle$, are negligibly small.

The velocity gradient plays an essential role in the mean-flow dynamics. This paper introduces the nondimensional mean velocity gradient, $\Phi(z) = (\kappa z/u_*)(d\langle u \rangle/dz)$, which is equal to unity for the logarithmic profile (Fig. 1, dashed line). The derivative is estimated by the second-order central finite-difference method. Near the ground ($z/H \lesssim 0.05$) and at the top ($z/H \gtrsim 0.95$), the simulation value of Φ departs significantly from the log profile. This log-layer mismatch (also referred to as overshooting) problem near the ground is well known in LES simulations. Near the top, a large z-component of the velocity gradient is rarely mentioned and is in contradiction to the imposed slip boundary condition ($du/dz = 0$).

Velocity Variances and Reynolds Stresses

The velocity variance in the streamwise direction is much higher than in the other two directions, and the fluctuations are largest near the ground. The shape and magnitude of the profiles (Fig. 2) are consistent with the analytical expressions from the similarity theory (Stull 1988) and results in Porté-Agel et al. (2000), Andren et al. (1994), and Brost et al. (1981). The decrease in magnitude near the ground is not attributable to the molecular viscosity effect but mainly to the strong SGS dissipation, which extracts energy from the filtered motions and moves it to the SGS motions.

The total stresses in the streamwise direction are balanced by the external pressure gradient, varying linearly with height as $u_*^2(z/H - 1)$. Because the molecular viscosity is negligible, the sum of Reynolds and SGS stress is a linear function of z. The sum of the normalized mean Reynolds and SGS stress in the streamwise direction is in agreement within 95% with the theoretical profile (the solid line) at $z/H \gtrsim 0.05$. The SGS stress is too large near the ground because of the inaccuracy of SGS model.

Velocity Spectra

For neutrally stratified ABL flows, the power spectrum of each velocity component follows approximately a model in the part of atmospheric boundary layer in which the logarithmic law holds (Simiu and Scanlan 1996), that is

$$\frac{nS_u}{u_*^2} = \frac{200f}{(1+50f)^{5/3}}, \quad \frac{nS_v}{u_*^2} = \frac{15f}{(1+9.5f)^{5/3}}, \quad \frac{nS_w}{u_*^2} = \frac{3.36f}{1+10f^{5/3}} \tag{1}$$

where n = frequency; u_* = friction velocity on the ground; $f = nz/\langle u \rangle$ = Monin coordinate; and $S_{u,v,w}$ = temporal spectra. In Fig. 3, the nondimensional temporal spectra of three velocity components are plotted as a function of nondimensional frequency f at $z/H = 0.1$. The temporal spectra agree with the typical expressions for the inertial subrange used in wind engineering. For most buildings, peak roof suctions occurring near eaves are strongly influenced by the effect of small-scale turbulence on the shape of flow separation layers.

The low-frequency spectrum deficit is a problem that arises not only in CFD simulations but also in the wind tunnel simulation of the atmospheric boundary layer flow, where it arises largely owing to limitations in the size of the wind tunnel. That deficit has little or no influence on the transport of momentum into the separation bubble. On the other hand, the fact that the effect of low-frequency turbulence on building response is quasi-static, rather than dynamic, allowed the development of approximate methods that account for

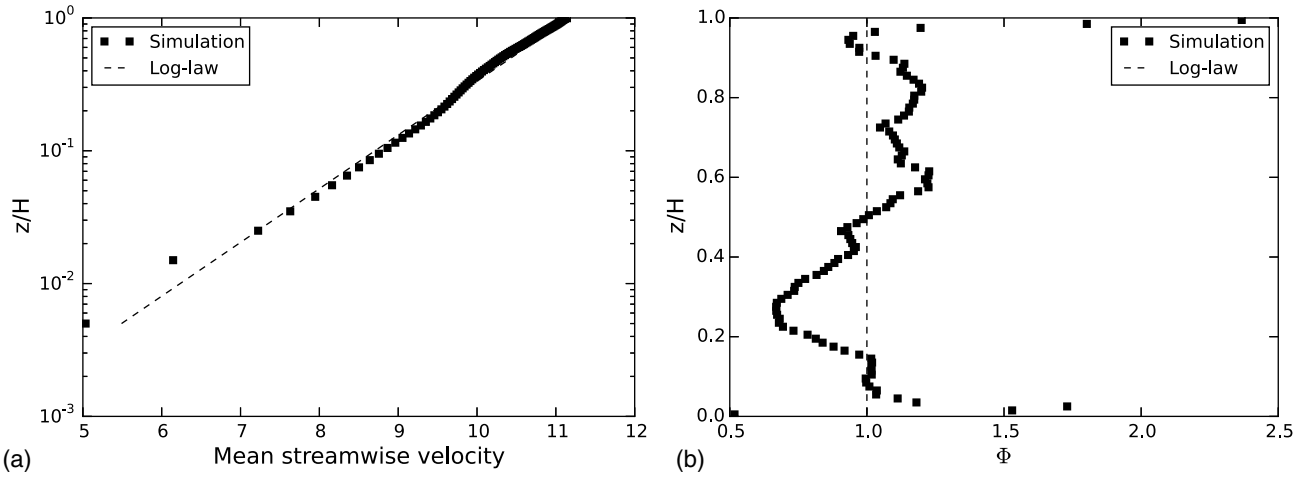

Fig. 1. (a) Vertical profiles of the mean streamwise velocity $\langle u \rangle$; (b) the nondimensional mean velocity gradient $\Phi = (\kappa z/u_*)(d\langle u \rangle/dz)$; the dashed lines are the logarithmic profiles

J. Eng. Mech., 2017, 143(9): 06017011

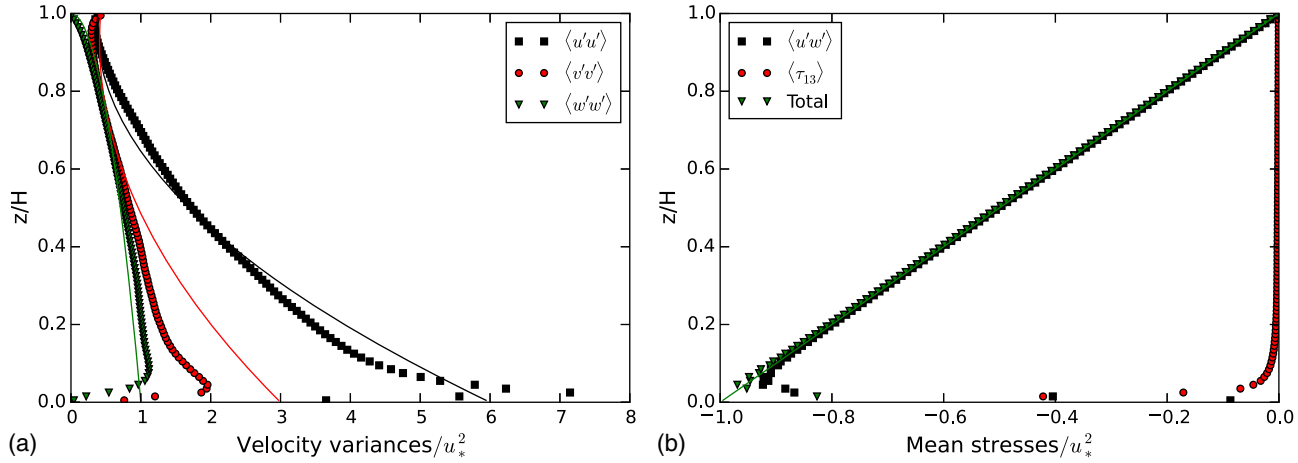

Fig. 2. (a) Vertical profiles of the normalized velocity variances; (b) Reynolds stresses; the solid lines are analytical expressions from similarity (Stull 1988) theory and from the force balance

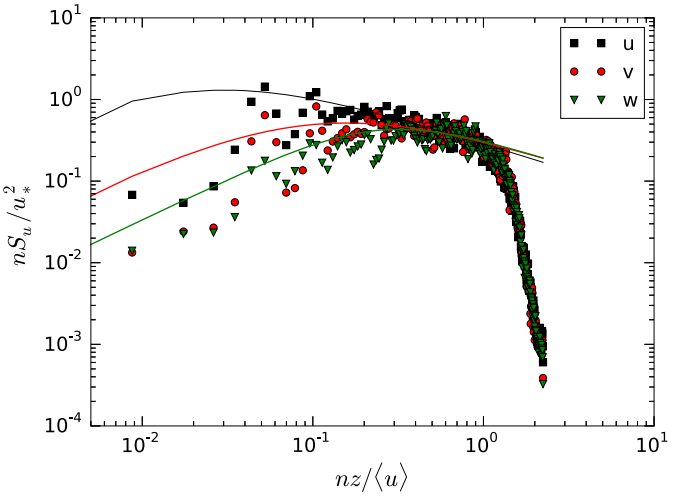

Fig. 3. Spectra of velocity components at the point $(x, y, z) = (H, 0.5H, 0.1H)$; the smooth thin lines are modified Kaimal expressions for spectra of u, v, and w

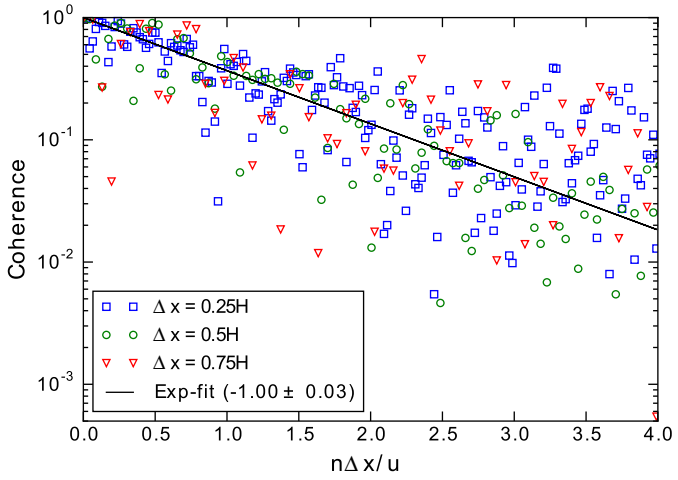

Fig. 4. Coherence function for two points in the x-direction; the points are at the height $z/H = 0.1$ and $\langle u \rangle$ is the mean of the streamwise velocities at two points; x-axis is nondimensional frequency; the number after the sign $\pm$ indicates the standard deviation errors from the exponential fittings

that effect in most practical cases (e.g., Yeo and Chowdhury 2013). The method consists of conservatively substituting for the missing low-frequency content, a zero-frequency fluctuation (i.e., an increment of the mean speed) with amplitude equivalent to the contribution of that content to the response. A more elaborate method is described in Mooneghi et al. (2016). These methods can also be used in a CFD context.

Spatial Coherence of Streamwise Velocity

The spatial coherence of streamwise velocity is evaluated to estimate the characteristic size of turbulent structures. The cross-spectrum $S_{u_1u_2}$ of two points is the Fourier transform of the cross-covariance and is a complex quantity consisting of a symmetric part $S^C_{u_1u_2}$ and an antisymmetric part $S^Q_{u_1u_2}$, namely, $S_{u_1u_2} = S^C_{u_1u_2} + iS^Q_{u_1u_2}$. The coherence of two signals is defined as

$$\gamma^2_{u_1u_2}(\Delta r, n) = \frac{(S^C_{u_1u_2})^2 + (S^Q_{u_1u_2})^2}{S_{u_1u_1}S_{u_2u_2}} \tag{2}$$

The coherence is a function of the distance between the two points Δr, the frequency n, and the mean velocities at the elevations of the two points. The square root of the coherence can be approximated by an exponential function, for example in the x-direction, $\gamma_{u_1u_2} \simeq e^{-c_{\gamma x} n \Delta x/\langle u \rangle}$, in which $c_{\gamma x}$ is the exponential decay coefficient for the x-direction.

In Fig. 4, the coherence function, with the frequency normalized by $\langle u \rangle/\Delta x$, for two points at the same height but separated by distance Δx in the x-direction is plotted. The fitted exponential decay coefficient is $c_{\gamma x} \simeq 1.00 \pm 0.03$. Similar procedures are applied for the y- and z-direction, for which the functions are both exponential, and the exponential decay coefficients are fitted to be $c_{\gamma y} \simeq 14.09 \pm 0.42$ and $c_{\gamma z} \simeq 11.46 \pm 0.44$, respectively. The fitted values in this study are obtained at height $z/H = 0.1$.

Conclusions

A wall-modeled LES study of turbulent ABL flow is presented for structural engineering applications based on the open-source toolbox *OpenFOAM*. LES simulations were performed in a rectangular parallelepiped computational domain with a uniform cubic-grid mesh. Periodic boundary conditions were applied in the horizontal directions, whereas slip boundary condition was

imposed at the top, and no-slip on the ground for the velocity. A wall stress model was used to ensure the correct surface stress on the ground. Initial perturbations of wavy flow structures were introduced to reduce the initial relaxation time.

Except for the mismatch near the ground, the mean velocity and velocity gradient profiles followed reasonably well the logarithmic law. The second-order moments of turbulence were in good agreement with previous studies. The temporal spectra are in good agreement with expressions commonly used in wind engineering applications. The spatial coherence functions are exponential, and the fitting decay exponential coefficient in the x-direction is much smaller than in the y- and z-directions, which indicates streamwise elongated turbulent structures as observed in the simulations.

Although reasonable accuracy is achieved in the bulk flow, challenges on LES of boundary layer flows still remain near the wall. Some prominent, persisting problems exist, such as the log-layer mismatch near the ground. Extensive tests showed that the mismatch is mainly a result of the limited accuracy of the SGS model, because the flow near the ground violates the isotropic assumption of the SGS model. Further research efforts will be invested on the improvement in *OpenFOAM* of the SGS model near solid walls.

Acknowledgments

Dr. E. Simiu served as project leader. Mr. Paul Dickey's excellent technical support is gratefully acknowledged.

References

Andren, A., et al. (1994). "Large-eddy simulation of a neutrally stratified boundary layer: A comparison of four computer codes." *Q. J. R. Meteorolog. Soc.*, 120(520), 1457–1484.

Brost, R. A., Wyngaard, J. C., and Lenschow, D. H. (1981). "Marine stratocumulus layers. II: Turbulence budgets." *J. Atmos. Sci.*, 39(4), 818–836.

Courant, R., Friedrichs, K., and Lewy, H. (1928). "Über die partiellen differenzengleichungen der mathematischen physik." *Math. Ann.*, 100(1), 32–74 (in German).

Crank, J., and Nicolson, P. (1947). "A practical method for numerical evaluation of solutions of partial differential equations of the heat conduction type." *Math. Proc. Cambridge Philos. Soc.*, 43, 50–67.

Jasak, H. (1996). "Error analysis and estimation for the finite volume method with applications to fluid flows." Ph.D. thesis, Imperial College of Science, Technology and Medicine, London.

Mooneghi, M. A., Irwin, P., and Chowdhury, A. G. (2016). "Partial turbulence simulation method for predicting peak wind loads on small structures and building appurtenances." *J. Wind Eng. Ind. Aerodyn.*, 157, 47–62.

Porté-Agel, F., Meneveau, C., and Parlange, M. B. (2000). "A scale-dependent dynamic model for large-eddy simulation: Application to a neutral atmospheric boundary layer." *J. Fluid Mech.*, 415, 261–284.

Schumann, U. (1975). "Subgrid scale model for finite difference simulations of turbulent flows in plane channels and annuli." *J. Comput. Phys.*, 18(4), 376–404.

Shi, L., and Yeo, D. (2016). "OpenFOAM large-eddy simulations of atmospheric boundary layer turbulence for wind engineering applications." National Institute of Standards and Technology, Gaithersburg, MD, 1–32.

Simiu, E., and Scanlan, R. H. (1996). *Wind effects on structures*, Wiley, New York.

Stull, R. B. (1988). *An introduction to boundary layer meteorology*, Kluwer, Dordrecht, Netherlands.

OpenFOAM 2.4.0 [Computer software]. OpenFOAM, London.

Yeo, D., and Chowdhury, A. G. (2013). "Simplified wind flow model for the estimation of aerodynamic effects on small structures." *J. Eng. Mech.*, 10.1061/(ASCE)EM.1943-7889.0000508, 367–375.